Cancer Research

KDM4 Inhibition Targets Breast Cancer Stem–like Cells

Eric Metzger[1], Stella S. Stepputtis[2,3], Juliane Strietz[2], Bogdan-Tiberius Preca[2], Sylvia Urban[1], Dominica Willmann[1], Anita Allen[1], Fides Zenk[4], Nicola Iovino[4], Peter Bronsert[3,5], Amelie Proske[6], Marie Follo[7], Melanie Boerries[3,8], Elmar Stickeler[9], Jiangchun Xu[10], Michael B. Wallace[10], Jeffrey A. Stafford[10], Toufike Kanouni[10], Jochen Maurer[2,3], and Roland Schüle[1,3,11]

Abstract

Traditional treatments for breast cancer fail to address therapy-resistant cancer stem–like cells that have been characterized by changes in epigenetic regulators such as the lysine demethylase KDM4. Here, we describe an orally available, selective and potent KDM4 inhibitor (QC6352) with unique preclinical characteristics. To assess the antitumor properties of QC6352, we established a method to isolate and propagate breast cancer stem–like cells (BCSC) from individual triple-negative tumors resected from patients after neoadjuvant chemotherapy. Limiting-dilution orthotopic xenografts of these BCSCs regenerated original patient tumor histology and gene expression. QC6352 blocked BCSC proliferation, sphere formation, and xenograft tumor formation. QC6352 also abrogated expression of EGFR, which drives the growth of therapy-resistant triple-negative breast cancer cells. Our findings validate a unique BCSC culture system for drug screening and offer preclinical proof of concept for KDM4 inhibition as a new strategy to treat triple-negative breast cancer. *Cancer Res; 77(21); 5900–12. ©2017 AACR.*

Introduction

Breast cancer is the leading cause of cancer-related death among women worldwide (1). Among the subtypes of breast cancer, triple-negative disease is associated with a particularly poor prognosis and limited therapeutic options (2). During breast cancer treatment, therapy resistance and metastatic dissemination are the main problems that have to be faced (1). Of note, breast cancer stem cells (BCSC) have been suggested to be responsible for both therapy resistance and metastatic dissemination (3, 4). Until now, these resistant cancer stem cell populations have only been poorly characterized and targeted therapeutics have yet to be identified.

It has been shown that alterations of epigenetic regulators such as the KDM4 family members control tumor cell proliferation particularly in aggressive breast cancers (5) and dysregulation of KDM4 demethylases has been documented in a variety of cancers including breast cancer (6). The KDM4 subfamily is comprised of KDM4A, B, C, and D and belongs to the Jumonji C (JmjC) domain-containing family of histone demethylases (7). KDM4 demethylases catalyze removal of the repressive H3K9me3 mark and that of H3K36me3, a mark linked to transcriptional elongation (8), thereby regulating a range of crucial pathways. These findings highlight KDM4 demethylases as potential therapeutic targets for breast cancer treatment. Consequently, we set out to test potent and selective drug-like KDM4 inhibitors. In order to validate inhibitors on cancer stem cells (CSC) from triple-negative breast cancer (TNBC), we established an efficient three-dimensional (3D) cultivation method allowing for growth of CSCs from patient tumor tissue without prior fluorescence-activated cell sorting (FACS) or murine xenografts to enrich for CSCs. We used defined conditions including a serum-free culture medium, a rho kinase inhibitor, Matrigel, and a low oxygen environment to isolate and enrich for BCSCs from individual patient tumors after neoadjuvant chemotherapy.

Materials and Methods

Tissue specimens

All patients were operated at the Department of Obstetrics and Gynecology at the University Medical Centre Freiburg. Tumor

[1]Urologische Klinik und Zentrale Klinische Forschung, Universitätsklinikum Freiburg, Medizinische Fakultät, Albert-Ludwigs-Universität Freiburg, Freiburg, Germany. [2]Department of General and Visceral Surgery and Comprehensive Cancer Center, University Medical Center Freiburg, Freiburg, Germany. [3]Deutsches Konsortium für Translationale Krebsforschung, Standort Freiburg, Freiburg, Germany. [4]Department of Chromatin Regulation, Max Planck Institute of Immunobiology and Epigenetics, Stübeweg and University of Freiburg, Freiburg, Germany. [5]Department of Surgical Pathology, University Medical Center Freiburg, Freiburg, Germany. [6]Department of Hematology/Oncology, University Medical Center Freiburg, Freiburg, Germany. [7]Department of Internal Medicine I, University Medical Center Freiburg, Freiburg, Germany. [8]Institute of Molecular Medicine and Cell Research, University of Freiburg, Freiburg, Germany. [9]Department of OBGYN, University Clinic Aachen (UKA), Aachen, Germany. [10]Celgene Quanticel Research, San Diego, California. [11]BIOSS Centre for Biological Signalling Studies, University of Freiburg, Freiburg, Germany.

Note: Supplementary data for this article are available at Cancer Research Online (http://cancerres.aacrjournals.org/).

E. Metzger and S.S. Stepputtis contributed equally to this article.

J. Maurer and R. Schüle contributed equally to this article.

Corresponding Authors: Roland Schüle, Urologische Klinik und Zentrale Klinische Forschung, Universitätsklinikum Freiburg, Medizinische Fakultät, Albert-Ludwigs-Universität Freiburg, Breisacherstrasse 66, 79106 Freiburg, Germany. Phone: 49-761-270-63100; Fax: 49-761-270-63110; E-mail: roland.schuele@uniklinik-freiburg.de; and Jochen Maurer, Department of General and Visceral Surgery and Comprehensive Cancer Center University Medical Center Freiburg, Breisacher Str. 115, 79106 Freiburg, Germany. Phone: 49-761-270-63570; E-mail: jochen.maurer@uniklinik-freiburg.de

doi: 10.1158/0008-5472.CAN-17-1754

tissue specimens for BCSC isolation and paraffin embedding were obtained from pathologists of the tumor bank of the Comprehensive Cancer Centre Freiburg. All experiments were performed in accordance with the Declaration of Helsinki. We confirm that all experimental protocols were approved by the Institutional Review Board in the Ethics vote 307/13 (independent Ethics Committee University of Freiburg). Written informed consent was obtained from each patient.

BCSC isolation method

All primary breast cancer tumors were collected from individuals who had received chemotherapy and were classified as triple-negative. Primary BCSC lines were isolated by mechanical dissociation of the tumor material followed by enzymatic digestion in 5 mL DPBS (Gibco) supplemented with 6 units DNAse I (Machery-Nagel) and 1 mg liberase (Roche) for 1 h at 37°C. Afterward, the digestion medium was diluted with 10 mL DPBS and filtered through a cell strainer (40 μm, BD). Following centrifugation at 200 $\times g$ for 5 minutes, the supernatant was discarded and the cell pellet was washed with MEBM (Gibco). Subsequently, if red blood cells were visible in the pellet, 2 mL ACK Lysis-buffer (Gibco) was added to the cell pellet. After 1 minute of incubation at room temperature, the suspension was filled up to 6 mL with MEBM and centrifuged at 200 $\times g$ for 5 minutes. The supernatant was discarded and the pellet was resuspended in 1 mL MEBM and filtered through a 40-μm strainer. Following centrifugation at 200 $\times g$ for 5 minutes, the supernatant was discarded and the remaining cell pellet suspended in MSC medium. Isolated cells were counted and 2×10^4 cells in 200 μL of a 1:1 mixture of MSC medium and Matrigel (ice cold, Corning, 354230) were plated per well in a 24-well low attachment plate (Corning). After solidification of the Matrigel at 37°C for 30 minutes, each well was topped up with 500 μL of MSC medium. The cells were cultured at 37°C under low oxygen conditions (3% O_2, 5% CO_2, 92% N_2). 3D cells stably proliferating cells were cultured and expanded in 2D. All primary BCSC lines were isolated in 2014 and authenticated by the high-throughput Multiplex human cell authentification test (MCA) developed at the DKFZ in 2016 (9). *Mycoplasma* tests were conducted every 3 months via PCR detection utilizing the positive control provided free of charge by the Leibniz-Institute DSMZ. Experiments with cells were conducted in a passaging window of 15 passages.

MSC medium

The mammary stem cell (MSC) medium is composed of mammary epithelial basal medium (Gibco, 31331-028), supplemented with 1 × B27 (Gibco, 17504-044), 1 × amphotericin B (Sigma-Aldrich, A2942), and 1 × penicillin–streptomycin (Gibco, 15140122). Furthermore, epidermal growth factor (20 ng/mL, PeproTech, AF-100-15), heparin (4 μg/mL, Sigma-Aldrich, H3149), fibroblast growth factor (20 ng/mL, PeproTech, AF-100-18B), gentamicin (35 μg/mL, Gibco, 15750-045), and rho kinase inhibitor (500 nmol/L, Calbiochem, 555552) were added.

Cell culture

BCSCs were cultured as spheres in a 3D environment as described above. One milliliter medium was added after 2 days. Cells were split once a week using Dispase (Corning) to solve residual Matrigel and Accutase for sphere dissociation. To expand BCSCs in a 2D environment, 4×10^5 cells were seeded in 2 mL MSC medium containing 2% Matrigel (ice-cold) in a 10 cm culture dish. After solidification of the Matrigel at 37°C for 30 minutes, the dish was topped up with 8 mL of MSC medium. Cells were grown under low oxygen conditions as described above. Medium was changed after 3 days. Cells were split once a week.

Anchorage-independent cancer stem cell sphere assay in methylcellulose

Cells were detached by Accutase and counted. A total of 3×10^3 single BCSC1 and 1×10^3 single BCSC2 cells were seeded into individual wells of 96-well ultra-low attachment plates (Corning, 3474) in serum-free MSC medium containing 1% methylcellulose (Sigma, M0512). After 7 days, all spheres were counted to evaluate the sphere-forming capacity except for experiments including QC6352 treatment, where only spheres over 50-μm diameter were counted.

Cancer stem cell sphere assay in Matrigel

Cells were detached by Accutase and counted. Single BCSC1 and BCSC2 cells (1×10^3) were seeded as triplicates in 50% Matrigel into individual wells of 24-well ultra-low attachment plates (Corning) in serum-free MSC medium. QC6352 and QC6688 were dissolved in DMSO and paclitaxel in 0.9% saline solution. After 7 days, spheres over 50 μm diameter were counted for QC6352- and QC6688-treated and control cells and spheres over 20 μm diameter were counted for paclitaxel-treated and control cells. For the assessment of secondary sphere formation, wells with 4×10^4 single BCSC1 and BCSC2 spheres were seeded and treated as described above. After 7 days, BCSC1 and BCSC2 cells were split and counted as described above. From these, 1×10^3 single BCSC1 and BCSC2 cells were seeded in triplicates as described above to assess secondary sphere formation in the absence of QC6352, QC6688 or paclitaxel. After 7 days, spheres over 50 μm diameter were counted for QC6352- and QC6688-treated and control cells, and spheres over 20 μm diameter were counted for paclitaxel-treated and control cells.

Cell proliferation assay

High titer lentiviral stock (CMV-NLS-mCherry) was obtained from the Sanford Burnham Prebys Medical Discovery Institute. Lentiviral particles were added at a multiplicity of infection (MOI) of 5 to BCSC1 and BCSC2 in MSC medium. Cells were cultured as described. For cell proliferation assay, BCSC1mCherry and BCSC2mCherry were detached by Accutase and counted. 384-well plates (Greiner, 781091) were coated with 10 μL of MSC medium containing 2% of Matrigel (Corning, 354230). After incubation at 37°C for 30 minutes to solidify the Matrigel, 1×10^3 single cells were seeded per well in 384-well. Inhibitor was added 24 hours later to the indicated final concentrations. Subsequently, daily cell number assessment for the indicated number of days was performed utilizing the ScanR microscope-based imaging platform (Olympus) and ScanR software 6. At each time point, mCherry-positive cell nuclei in 9 sectors of each well were assessed with a 10× lens.

Adenoviral knockdown of KDM4 isoforms

High titer adenoviral stocks (shRNA Ctrl (Ad-GFP-U6-scrambled-shRNA; #1122N), shRNA KDM4A (Ad-GFP-U6-h-KDM4A-shRNA; #shADV-212841), shRNA KDM4B (Ad-GFP-U6-h-KDM4B-shRNA; #shADV-212842), shRNA KDM4C (Ad-GFP-U6-h-KDM4C-shRNA; #shADV-212844), and shRNA

KDM4D [Ad-GFP-U6-h-KDM4D-shRNA(#70); #shADV-212848)] were obtained from Vector BioLabs. Adenoviral particles were added at an MOI of 300 to BCSC1 cells and MOI of 150 to BCSC2 cells in MSC medium. Cells were harvested 3 days after infection for Western blot analyses and after 5 days for Chromatin immunoprecipitation (ChIP) and ChIP-seq analyses. For cell proliferation assays, BCSC1 were infected with an MOI of 300. After 5 days, BCSC1 were seeded into 384-well plates and reinfected with an MOI of 300. To generate xenografts, BCSC1 were infected with an MOI of 300. After 24 hours, BCSC1 were detached, reinfected with an MOI of 300 and 1×10^5 cells transplanted into immunocompromised mice as described below.

ChIP

ChIP experiments were performed essentially as previously described (10). BCSC1 cells were either cultured for 18 hours in the absence or presence of 5×10^{-8} mol/L QC6352 or cells were infected 5 days before harvesting with adenovirus expressing either shRNA against KDM4A or scrambled control shRNA (Ad-GFP-U6-hKDM4A-shRNA and Ad-U6-RNAi-GFP, respectively, Vector Biolabs) according to the manufacturer's instructions. Immunoprecipitation was performed with specific antibodies (anti-KDM4A (#5766, lot 021110, Schuele Laboratory), anti-H3K9me3 (Diagenode, #C15410056, lot A1675-001P), anti-H3 (#ab1791, lot GR300976-1, Abcam), spike-in antibody (#61686, Active Motif), rIgG (#C15410206, lot RIG001L, Abcam) in the presence of spike-in chromatin (#53083, Active Motif) on GammaBind G-Sepharose (GE-Healthcare). For PCR, 2 μL out of 70 μL isolated DNA were used. Primer sequences were as follows: *EGFR* 5′-cagagctcatcctggccaac-3′ and 5′-ttctgtctgcacacttggca-3′. Libraries were prepared from immunoprecipitated DNA according to standard methods. ChIP-seq libraries were sequenced using a HiSeq 2000 (Illumina) and mapped to the hg19 reference genome using bowtie 2 (11). Data were further analyzed with the peak finding algorithm MACS 1.42 (12) using input as control. Normalization to spike-in chromatin was performed according to Ref (13). All peaks with FDR greater than 0.5% were excluded from further analysis. The uniquely mapped reads were used to generate the genome-wide intensity profiles, which were visualized using the IGV genome browser (14). HOMER (15) was used to annotate peaks, to calculate overlaps between different peak files, and for motif searches. The genomic features (promoter, exon, intron, 3′UTR, and intergenic regions) were defined and calculated using Refseq and HOMER. Data are deposited under GSE95294.

Orthotopic breast cancer xenografts

All animal studies and experiments were performed in accordance with German Animal Welfare regulations and in accordance with an Institutional Animal Care and Use Committee as described in the animal protocol G13/114. NOD/SCID females (4–5 weeks old) were anesthetized using an isoflurane inhalator. A small sagittal incision (no longer than 1.0 cm) on the shaved and sterilized abdomen allowed access to the mammary gland #4 on both sides. Indicated numbers of BCSCs were mixed with 1×10^6 irradiated fibroblasts [newborn human foreskin fibroblasts (NuFF), p11, GlobalStem, GSC-3002] and suspended in a 1:1 mixture of Matrigel (Corning, 354230) and MSC medium in a total volume of 40 μL per gland. The mixture was injected into the mammary fat pad of the #4 gland on both sides of the animal. Each transplant was localized distal to the lymph node in the gland. Surgical incisions were sealed by suturing with a 5/0 thread (Ethicon, Z995). Animals were monitored twice weekly for weight and tumor growth, which was determined by caliper measurement. Tumor volumes were calculated using the formula $4/3 \times \pi \times r^3$.

Ultrasonic 3D tumor model

Ultrasound measurements of xenograft tumors in NOD/SCID mice were performed using a small animal high-resolution ultrasound system (Vevo3100) and transducer (MX550D) with 40 MHz (VisualSonics). For 3D tumor modeling, the transducer was moved along the tumor automatically with a step size of 0.076 mm. Tumors were visualized with Vevo LAB (Version 1.7.1) at start and end of treatment.

In vivo treatment with QC6352

Immediately before treatment, QC6352 was dissolved in 50% polyethylene glycol (Sigma-Aldrich)/50% DPBS (pH 9, Gibco) with sonication (Diagenode bioruptor) until a clear solution was formed. When tumors reached a palpable size of 3 mm^3, mice were treated with vehicle (control) or QC6352. The inhibitor was administered daily to mice via oral gavage at 10 mg/kg. Control animals received vehicle only. Animals were monitored twice weekly for weight and tumor growth.

Dose–response assay

Cells were detached by Accutase, dissociated and counted. The wells of a black 384-well plate (Greiner) were coated with 10 μL of MSC medium containing 2% of Matrigel (354230, Corning). After incubation at 37°C for 30 minutes, to solidify the Matrigel, 1×10^3 single cells were seeded as described above. The inhibitor was added 24 hours later. Following 96 hours of incubation, cells were washed with DPBS and fixed with ice-cold methanol for 15 minutes at −20°C. Cells were washed with DPBS, stained with DAPI, and counted using the ScanR microscope-based imaging platform (Olympus).

Microarray analysis

Total RNA was isolated from patient tumor material, xenografts, and cells using the Universal RNA Purification Kit (Roboklon) according to the manufacturer's instructions. Isolated RNAs were processed with the Ambion WT Expression Kit (Ambion) as described by the manufacturer and hybridized to Illumina HT-12 v4 Expression Bead Chips following the standard Illumina protocols. Expression data were processed and quantile normalized using the R Bioconductor Beadarray package (16) in version 2.22. Only probesets mapping to an Entrez ID applying the Bioconductor package illuminaHumanv4.db (Version 1.26) were considered for further downstream analysis. In case of multiple probesets matching the same Entrez ID, we selected the probeset having the highest interquartile range across all samples. The dendrogram depicts a complete-linkage hierarchical clustering based on the Euclidean distance between the samples. Data are deposited under GSE95042.

Flow cytometry

To analyze the expression of established CSC markers, cells were detached and counted as described above. Cells (1×10^5) were washed with staining buffer (DPBS + 1% BSA) and stained for 20 minutes at room temperature in the dark with the following antibodies diluted in staining buffer: anti-CD24 (eBioscience,

46-0247; 1:100), anti-CD44 (eBioscience, 12-0441-81; 1:1000), anti-EpCAM (eBioscience, 660 50-9326; 1:100), and anti-CD49f (eBioscience, 46-0495; 1:200). Cells were analyzed using BD LSR Fortessa and FlowJo software (Version 6).

Immunohistochemistry

Patient tumor tissue specimens were fixed in 10% formalin and embedded in paraffin. Two-μm-thick paraffin-embedded tissue sections were mounted onto glass slides. All slides were stored for two days at 58°C in a drying chamber, subsequently deparaffinized using xylene and hydrated with ethanol. Human and corresponding xenograft tumor tissue were stained using the following antibodies: anti-ER (clone EP1, code IR084, Dako); anti-PR (clone PgR 636, code IR068, Dako); anti-HER2 (code A0485, Dako); anti-Ki67 (clone MIB-1, code IR626, Dako); anti-vimentin (clone V9, code IR630, Dako); anti–E-cadherin (clone NCH-38, code IR059, Dako), and anti-cytokeratin 8/18 (clone EP17/EP30, code IR094, Dako). For the horseradish-based peroxidase detection EnVision Flex Peroxidase-Blocking Reagent (Dako, SM801), EnVision Flex+ Rabbit (LINKER; Dako, K8019) or EnVision Flex+ Mouse (LINKER; Dako, K8021) and EnVision Flex/HRP (Dako, SM802) were used. Counterstaining was performed with hemalum before adding a coverslip. As internal positive control, patient-derived physiological mammary gland was used for ER, PR, Ki67 (nuclear staining), cytokeratin 8/18 and E-cadherin (membranous, cytoplasmic staining). The mammary gland-surrounding myoepithelial layer was used as internal control for vimentin. For HER2, tissue specimens from HER2-positive breast cancer patients (score 3 according to ref. 17) were included for every HER2 staining session as external positive control. TNBC was defined as ER-, PR-, and HER2-negative (score < 2; ref. 18).

Western blot analysis

Experiments were performed as previously described (10). The following antibodies were used: anti-KDM4A (#5766, lot 021110, Schuele Laboratory), anti-KDM4B (#4662, lot 962009, Schuele Laboratory), anti-KDM4C (#23855, lot 23062015, Schuele Laboratory), anti-KDM4D (#ARP35946, lot 001, Aviva Systems Biology), anti-EGFR (#2232S, lot 16, Cell Signaling Technology).

RNA preparation and analysis

Cells were cultured in the presence of vehicle or 5×10^{-8} mol/L QC6352. RNA was isolated as previously described (19). Quantitative RT-PCR was performed using the Abgene SYBR Green PCR Kit (Invitrogen) according to the supplier's protocol. *HPRT* was used for normalization. Primer sequences for *HPRT* were described previously (20). Other primers were as follows: *VCAN*: 5′-ACTGTGGATGGGGTTGTGTT-3′, 5′-CTGCGTCACACTGC TCAAAT-3′; *PRR5*: 5′-CGGGACAAGATTCGCTTCTA-3′, 5′-AGCGCATCC TCTAGCTTCAC-3′; *ATF4*: 5′-CCAACAACAGCAAGGAGGAT-3′, 5′-GTGTC ATCCAACGTGGTCAG-3′; *EGR1*: 5′-TGACCGCAGAGTCTTTTCCT-3′, 5′-CACAAGGTGTTGCCACTGTT-3′; *FST*: 5′-GGAAAACCTACCGCAATGAA-3′, 5′-GAGCTGCCTGGACAGAAAAC-3′; *EGFR*: 5′-CCAACCAAGCTCTCTTGA GG-3′, 5′-GCTTTCGGAGATGTTGCTTC-3′.

RNA sequencing

BCSC1 cells were cultured for 18 hours in the absence or presence of 5×10^{-8} mol/L QC6352. RNA was isolated as described above. RNA samples were sequenced by the standard Illumina protocol to create raw sequence files (.fastq files) at the sequencing core facility of the DKFZ. Reads were aligned to the hg19 build of the human genome using TopHat version 2 (21). The aligned reads were counted with the homer software (analyzeRNA) and DEG's were identified using EdgeR (22). Data are deposited under GSE95294.

Pharmacokinetic analyses

An intravenous dosing solution was made by dissolving QC6352 into phosphate buffered saline. The pH was adjusted to 9 by dropwise addition of 1 N NaOH. An oral dosing suspension was made by dissolving QC6352 into 0.5% methylcellulose. The intravenous and oral dosing solutions were administered at 5 and 10 mg/kg, respectively, to female CD-1 mice. Pharmacokinetic parameters were calculated as the average of groups consisting of three animal.

Statistical analyses

Data are represented as mean and SD or SEM as indicated. Significance was calculated by a two-tailed Student *t* test or one-way ANOVA as indicated with GraphPad Prism Version 6. *P* values below 0.05, 0.01, and 0.001 are indicated in figures as *, **, and ***, respectively.

Determination of the QC6352 IC_{50}

The ability of QC6352 to inhibit the activity of different KDM family members was determined in 384-well plate format under the following reaction conditions: 2 nmol/L enzyme, 300 nmol/L H3K9me3, H3K4me3, or H3K36me2 biotin-labeled peptides (Anaspec), 100 μmol/L alpha-ketoglutaric acid in assay buffer containing 50 mmol/L HEPES, pH 7.3, 0.005% Brij35, 0.5 mmol/L TCEP, 0.2 mg/mL BSA, 50 μmol/L sodium L-ascorbate, and 2 μmol/L ammonium iron(II) sulfate. Reaction product was determined quantitatively by TR-FRET after the addition of detection reagent phycolink streptavidin-allophycocyanin (Prozyme) and Europium-anti-H3K9me2, H4K4me2, or H3K36me1 antibody (PerkinElmer) in the presence of 5 mmol/L EDTA in LANCE detection buffer (PerkinElmer) at a final concentration of 50 nmol/L and 1 nmol/L, respectively. To initiate the assay reaction, 2 μL of 6 nmol/L enzyme and 2 μL of 11-point serially diluted QC6352 in 3% DMSO were added to each well for 60 minutes, followed by the addition of 2 μL of a mixture of 900 nmol/L biotin labeled peptide and 300 μmol/L α-ketoglutaric acid. After incubation at room temperature for 20 minutes, the reaction was terminated by addition of 6 μL of 5 mmol/L EDTA in LANCE detection buffer containing 100 nmol/L Phycolink streptavidin-allophycocyanin and 2 nmol/L europium-labeled antibody. After 60 minutes of incubation at room temperature, plates were read by EnVisionMultilabel Reader in TR-FRET mode (excitation at 320 nm, emission at 615 and 665 nm). A ratio was calculated (665/615) for each well and fitted to determine inhibition constant (IC_{50}).

Results

BCSC xenografts recapitulate original tumors of patients

As shown in Table 1, we established four BCSC lines (BCSC1-4), which originate from four independent breast tumor samples lacking estrogen receptor (ER), progesterone receptor

Table 1. Table representing data of original patient tumor, patient-derived cell lines BCSC1–4 and BCSC1–4–derived xenografts

		Patient tumor						Xenograft tumor				
ID	Source	Primary diagnosis	ER status	PR status	HER2 status	Classification	Neoadjuvantly administered chemotherapeutic drugs	Tumor formation	ER status	PR status	HER2 status	Classification
BCSC1	1° breast tumor	IC	Neg	Neg	Neg	Triple-negative	FEC, FAC, TAC, TC, cisplatin	36/38	Neg	Neg	Neg	Triple-negative
BCSC2	1° breast tumor	IDC	Neg	Neg	Neg	Triple-negative	Paclitaxel, doxorubicin	30/42	Neg	Neg	Neg	Triple-negative
BCSC3	1° breast tumor	IDC	Neg	Neg	Neg	Triple-negative	EC, docetaxel	13/13	Neg	Neg	Neg	Triple-negative
BCSC4	1° breast tumor	MC	Neg	Neg	Neg	Triple-negative	AC, paclitaxel, GemCa	7/8	Neg	Neg	Neg	Triple-negative

Abbreviations: ID, Identifier; BCSC1–4, breast cancer stem cell lines 1–4; IC, invasive carcinoma; IDC, invasive ductal carcinoma; MC, metaplastic carcinoma; ER, estrogen receptor; PR, progesterone receptor; HER2, human epidermal growth factor receptor 2; FEC, 5FU/epirubicin/cyclophosphamide; FAC, 5FU/doxorubicin/cyclophosphamide; TAC, docetaxel/doxorubicin/cyclo-phosphamide; TC, docetaxel/cyclophosphamide; EC, epirubicin/cyclophosphamide; AC, doxorubicin/cyclophosphamide; GemCa, gemcitabine/carboplatin.

(PR), and human epidermal growth factor receptor 2 (HER2) proteins. BCSCs could be cultivated in a 2D and 3D environment and grow as epithelial clusters and spheres, respectively (Fig. 1A and Supplementary Fig. S1A). *In vitro* clonogenic assays such as sphere formation assays have been developed to study proliferation, self-renewal, and differentiation of cell populations at the single-cell level (23). Thus, to verify their stem cell potential BCSC1 and BCSC2 were challenged in an anchorage-independent growth assay. BCSC1 and BCSC2 demonstrated a sphere-forming capacity of 10.8% and 16.2%, respectively, providing evidence for the potential of BCSC1 and BCSC2 to self-renew (Fig. 1B and Supplementary Fig. S1B). CSCs from breast cancer have been described to express specific surface markers such as CD49f, EpCAM, and CD44 while lacking expression of CD24 (24, 25). We analyzed BCSC1 and BCSC2 for these stem cell markers and found 58% $CD24^-/CD44^+$ and 96% $EpCAM^+/CD49f^+$ cells in BCSC1 and 5% $CD24^-/CD44^+$ and 97% $EpCAM^+/CD49f^+$ cells in BCSC2 (Fig. 1C and D; Supplementary Fig. S1C and S1D). The flow-cytometric analysis clearly showed that BCSC1 and BCSC2 harbor a stem cell population. To further corroborate the stem cell potential of the BCSCs we performed limiting dilution orthotopic xenografts in immunocompromised NOD/SCID mice, the current gold standard assay for self-renewing CSCs. As few as 1×10^3 BCSC1 and BCSC2 were able to form tumors demonstrating that both cell lines contain tumorigenic CSCs (Fig. 1E and F; Supplementary Fig. S1E). In summary, we used three independent methods namely sphere formation, flow cytometry analysis, and xenografts to demonstrate stemness, self-renewal capacity, and tumorigenicity of BCSC1 and BCSC2.

To further address the ability of these cells to regenerate the original patient tumor in a xenograft tumor model we analyzed tumors derived from BCSC1 and BCSC2 transplants histologically and genetically. Immunohistochemical analyses of BCSC1 and BCSC2 xenograft tumors using the mammary epithelial marker cytokeratin 8/18, E-cadherin, and vimentin as well as the proliferation marker Ki67 indicated that the xenograft tumors share a similar pattern with their parental patient tumors (Fig. 1G and Supplementary Fig. S1F). Matching the parental tumor, the BCSC xenografts were devoid of ER, PR, and HER2 protein expression (Table 1, Fig. 1H, and Supplementary Fig. S1G). Unsupervised hierarchical clustering analysis of RNA microarray data showed that the BCSC tumor xenografts share a close expression profile with the parental patient tumors, indicating preservation of the respective molecular tumor subtype (Fig. 1I). BCSC lines clustered within the corresponding host tumor and xenograft subtype depicting a close correlation between the three entities (Fig. 1I). Taken together, our data demonstrate that BCSCs can be isolated from TNBC patient tissue using optimized culture conditions and faithfully recapitulate the patient tumor in xenografts.

KDM4A controls proliferation and xenograft tumor growth of BCSC1

To evaluate the expression levels of the KDM4 family members in BCSC1 and BCSC2 we performed Western blot analysis. As shown in Fig. 2A, we detected robust expression of KDM4A in both BCSC1 and BCSC2. In contrast, expression levels of KDM4B, C, and D were more heterogeneous (Fig. 2A). To see whether KDM4s control proliferation of BCSC1 we performed adenoviral shRNA-mediated knockdown of KDM4A, B, C, and D in BCSC1 and monitored proliferation in real time. As shown in Fig. 2B,

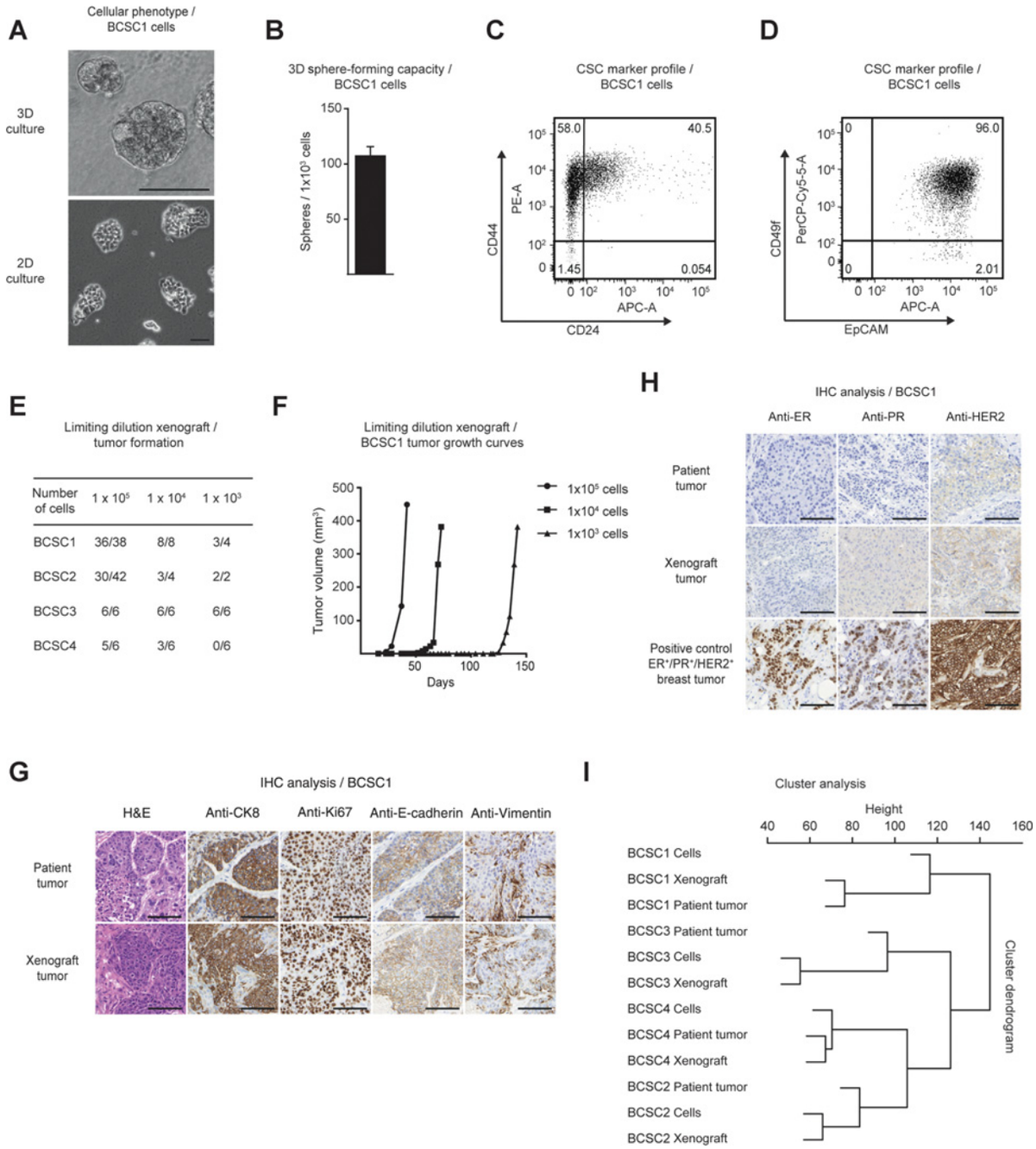

Figure 1.

BCSC xenografts recapitulate original tumors of patients. **A,** Representative pictures of BCSC1 cells cultured in 3D and 2D conditions. Scale bar, 100 μm. **B,** Sphere-forming capacity of BCSC1 cells in an anchorage-independent assay ($n = 3$). Data represent means + SEM. **C** and **D,** Expression pattern of CD24, CD44 (**C**), and EpCAM and CD49f (**D**) in BCSC1 cells analyzed by flow cytometry. **E,** Limiting dilution xenografts of BCSC1–4. **F,** Representative growth curves for limiting dilution assay of BCSC1 cell xenografts in immunocompromised mice. **G** and **H,** Hematoxylin and eosin (H&E) staining and immunohistochemical detection of CK8/18, Ki67, E-cadherin, and vimentin (**G**), and ER, PR, and HER2 (**H**) on representative sections of the original BCSC1 patient tumor and the BCSC1 xenograft tumor. Scale bar, 100 μm. **I,** Unsupervised hierarchical cluster analysis of RNA microarray data. Samples are original patient tumors, the tumor-derived BCSC1–4 lines, and the BCSC1–4 xenograft tumors derived from the BCSC lines 1–4.

depletion of KDM4A impaired proliferation of BCSC1 cells. In contrast, knockdown of KDM4B, C, or D did not influence proliferation of BCSC1 (Supplemental Fig. S2A–S2E).

Next, we wondered whether knockdown of KDM4A affects growth of BCSC1 xenografts. Therefore, BCSC1 were infected with adenovirus encoding either shRNA control (shRNA Ctrl) or

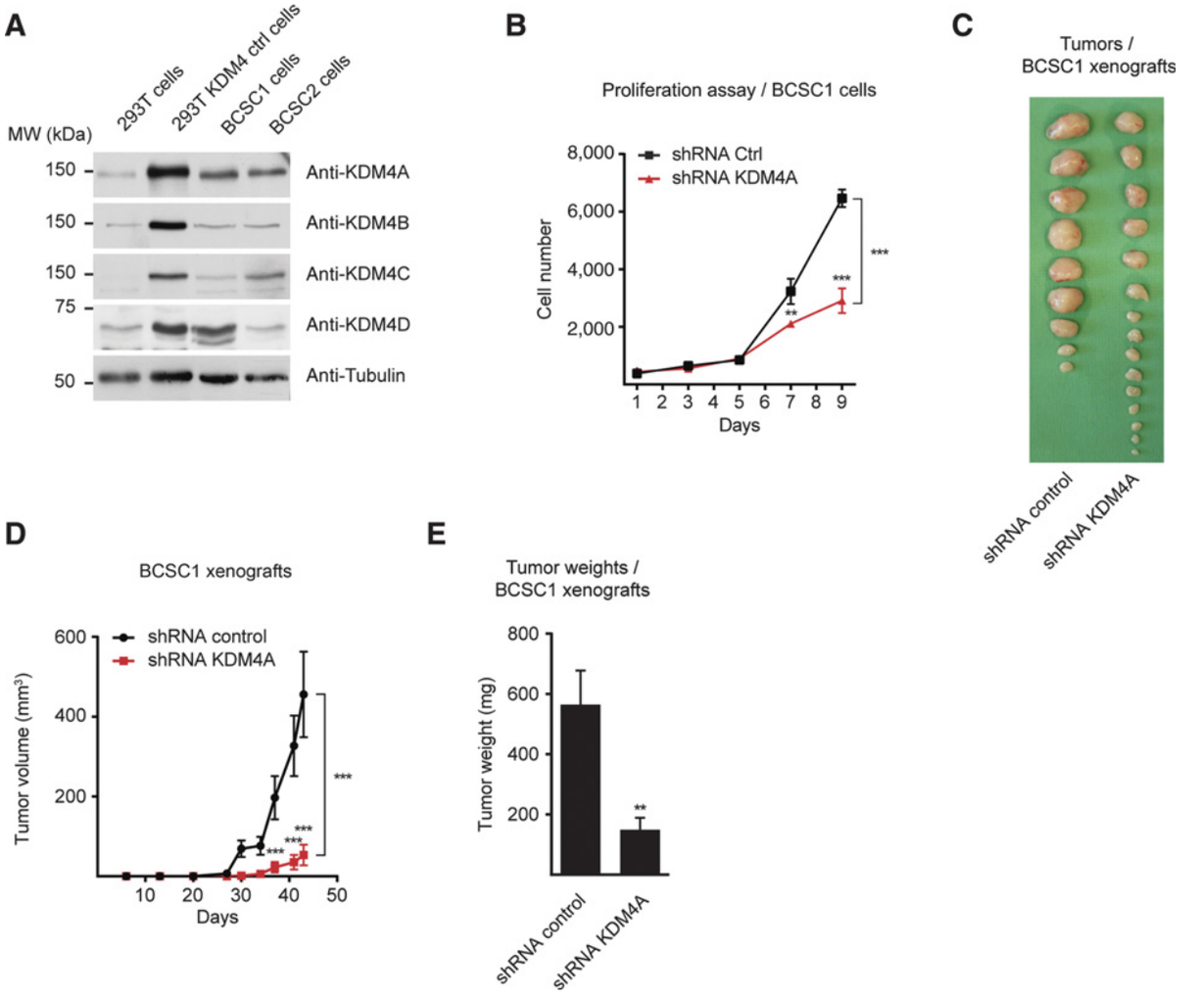

Figure 2.

KDM4A controls proliferation and xenograft tumor growth of BCSC1. **A,** Western blot analyses performed with anti-KDM4A, anti-KDM4B, anti-KDM4C, anti-KDM4D, and anti-tubulin antibodies. The samples are lysates from HEK293T, BCSC1, or BCSC2. HEK293T were transfected with expression plasmids for KDM4A, KDM4B, KDM4C, or KDM4D as indicated. **B,** Cell proliferation assay. BCSC1 were infected with adenoviruses coding for a control shRNA (shRNA Ctrl) or an shRNA against KDM4A (shRNA KDM4A; $n = 3$). Data represent means ± SD; **, $P < 0.01$; ***, $P < 0.001$ by one-way ANOVA. **C–E,** BCSC1-derived xenograft tumors grown for 43 days in mice. BCSC1 were infected with adenoviruses encoding either shRNA Ctrl or shRNA KDM4A. **C,** Representative BCSC1 xenograft tumors isolated from individual animals. **D,** Increase in tumor volume over time. Data represent means ± SEM; ***, $P < 0.001$ by one-way ANOVA. **E,** Final tumor weights of the BCSC1 xenografts. Data represent means + SEM; **, $P < 0.01$ by one-way ANOVA. For **C–E**, $n = 9$ (shRNA Ctrl), $n = 15$ (shRNA KDM4A).

shRNA against KDM4A (shRNA KDM4A) and implanted into the fat pads of immunocompromised NOD/SCID mice. Importantly, upon knockdown of KDM4A, tumor growth, and final tumor weight of the BCSC1-derived xenografts was strongly reduced (Fig. 2C–E). In contrast, the control knockdown of KDM4D (shRNA KDM4D) in BCSC1 did not significantly affect tumor growth and final tumor weight of the xenografts (Supplementary Fig. S2F–S2H). Together, our data demonstrate that the histone demethylase KDM4A controls proliferation and xenograft tumor growth of BCSC1. Furthermore, our bioinformatic analyses indicate that relapse-free survival over time decreases for patients with TNBC that express high levels of KDM4A in comparison to patients with TNBC that express low levels of KDM4A (Supplementary Fig. S2I). These findings indicate that targeting KDM4 might be a therapeutic option to limit expansion of BCSC populations.

QC6352 is a potent KDM4 inhibitor that blocks proliferation of BCSCs

Based on our observations that KDM4A controls proliferation and xenograft tumor growth of BCSC1 we decided to test whether the drug-like KDM4 inhibitor QC6352 (also called compound 6; ref. 26) might qualify for the treatment of BCSC-originating tumors (Fig. 3A). As a first step, prior to any investigation of either biological function or underpinning mechanism of action, we assessed the selectivity profile of the inhibitor. QC6352 was

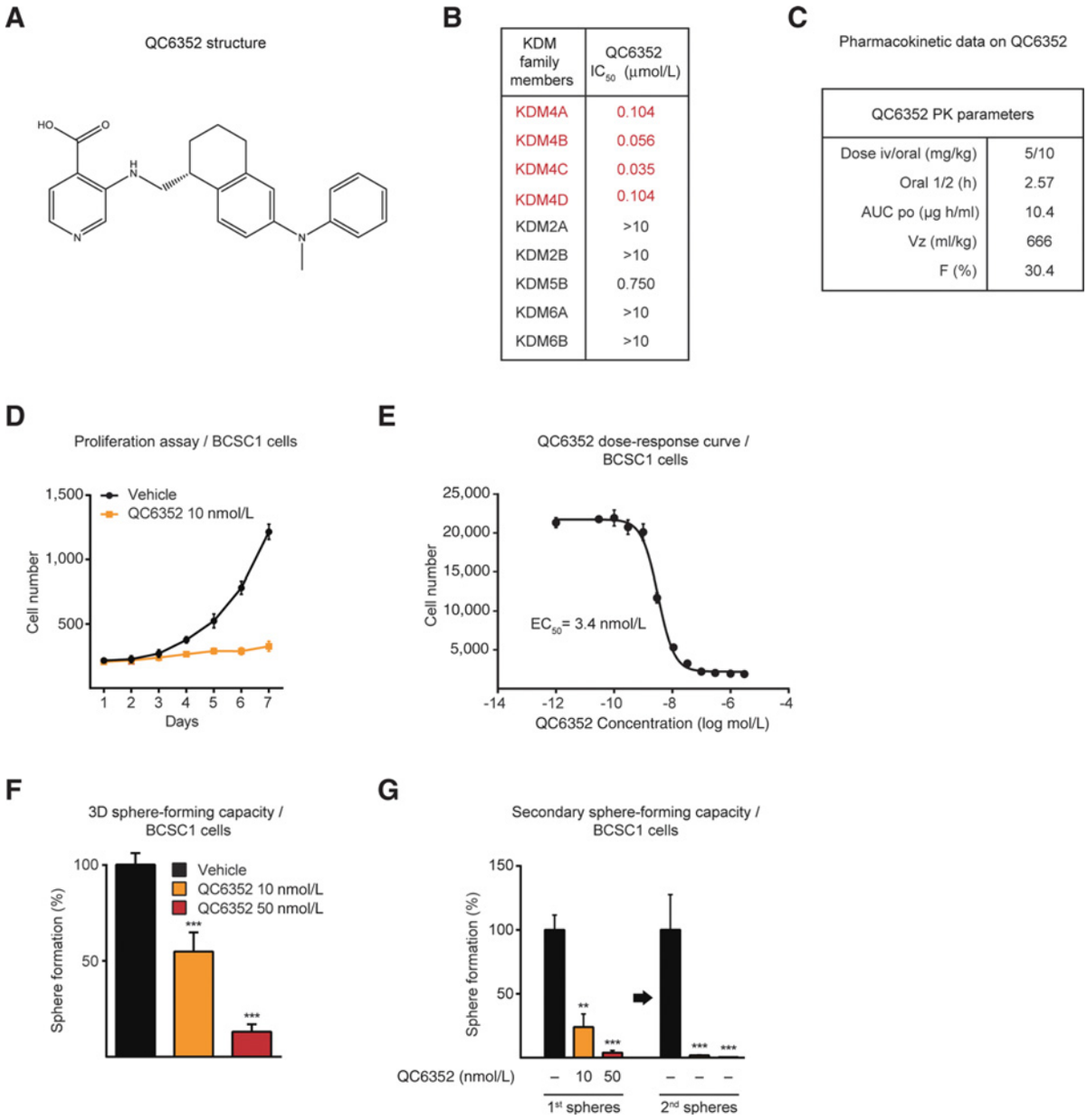

KDM family members	QC6352 IC_{50} (μmol/L)
KDM4A	0.104
KDM4B	0.056
KDM4C	0.035
KDM4D	0.104
KDM2A	>10
KDM2B	>10
KDM5B	0.750
KDM6A	>10
KDM6B	>10

QC6352 PK parameters	
Dose iv/oral (mg/kg)	5/10
Oral 1/2 (h)	2.57
AUC po (μg h/ml)	10.4
Vz (ml/kg)	666
F (%)	30.4

Figure 3.

QC6352 is a potent KDM4 inhibitor that blocks KDM4A-dependent proliferation of BCSC1. **A,** Structure of QC6352. **B,** Table depicting the half-maximal inhibitory concentration (IC_{50}) of QC6352 on different KDM family members. **C,** Pharmacokinetic properties of QC6352. iv, intravenous; AUC, area under the concentration–time curve; po, oral route; Vz, volume of distribution during terminal phase after intravenous administration; F, absolute bioavailability. **D,** Cell proliferation assay. BCSC1 were cultured in presence of vehicle or the indicated concentration of QC6352 ($n = 3$). **E,** Dose–response curve of QC6352 ($n = 3$). **F,** BCSC1 sphere formation in an anchorage-independent growth assay in presence of vehicle or the indicated concentrations of QC6352 ($n = 3$). **G,** Primary and secondary sphere formation of BCSC1 in Matrigel in the presence of vehicle or the indicated concentrations of QC6352 ($n = 3$). Data represent means ± SD (**D** and **E**) or means + SEM; **, $P < 0.01$; ***, $P < 0.001$ by one-way ANOVA (**F** and **G**).

evaluated against the KDM4 subfamily and other JmjC domain-containing histone demethylases such as KDM2A, 2B, 5B, 6A, and 6B. QC6352 inhibited the demethylase activity of KDM4A, B, C, and D at nanomolar concentrations with IC_{50} values between 35 and 104 nmol/L (Fig. 3B). QC6352 showed 100-to 300-fold selectivity over KDM2 and KDM6 demethylases and only weak inhibition of KDM5B (Fig. 3B). Finally, QC6352's favorable pharmacokinetic properties warranted further *in vivo* investigation (Fig. 3C). In summary, QC6352 presented as an orally available, potent, and selective KDM4 inhibitor.

When investigating the *in vitro* efficacy of QC6352 in BCSCs we observed that concentrations as low as 10 nmol/L inhibited

BCSC1 and BCSC2 cell proliferation (Fig. 3D and E; Supplementary Fig. S3A and S3B). To characterize and define the effect of QC6352 on stem cell potential (self-renewal and differentiation) we tested whether QC6352 treatment might interfere with the sphere-forming capacity of both BCSCs. Consequently, BCSCs were plated as single cells to ensure clonality and inspected for one week. In a concentration-dependent manner, QC6352 dramatically reduced the anchorage-independent sphere-forming capacity of BCSC1 and BCSC2 (Fig. 3F and Supplementary Fig. S3C). We then isolated single cells from 1 week QC6352-treated spheres and evaluated for anchorage-independent sphere formation in a secondary assay in the absence of QC6352. Of note, the secondary sphere-forming capacity was blocked even in the absence of inhibitor (Fig. 3G and Supplementary Fig. S3D). In contrast, the differentiation-inducing LSD1 inhibitor QC6688 (27) neither affected primary nor secondary sphere formation (Supplementary Fig. S3E and S3F). In addition, chemotherapeutics such as the taxane paclitaxel impaired proliferation of BCSC1 in primary sphere formation but did not interfere with stem cell potential and thus allowed secondary sphere formation (Supplementary Fig. S3G). Taken together, our data demonstrate that QC6352 blocks proliferation and self-renewal of BCSCs.

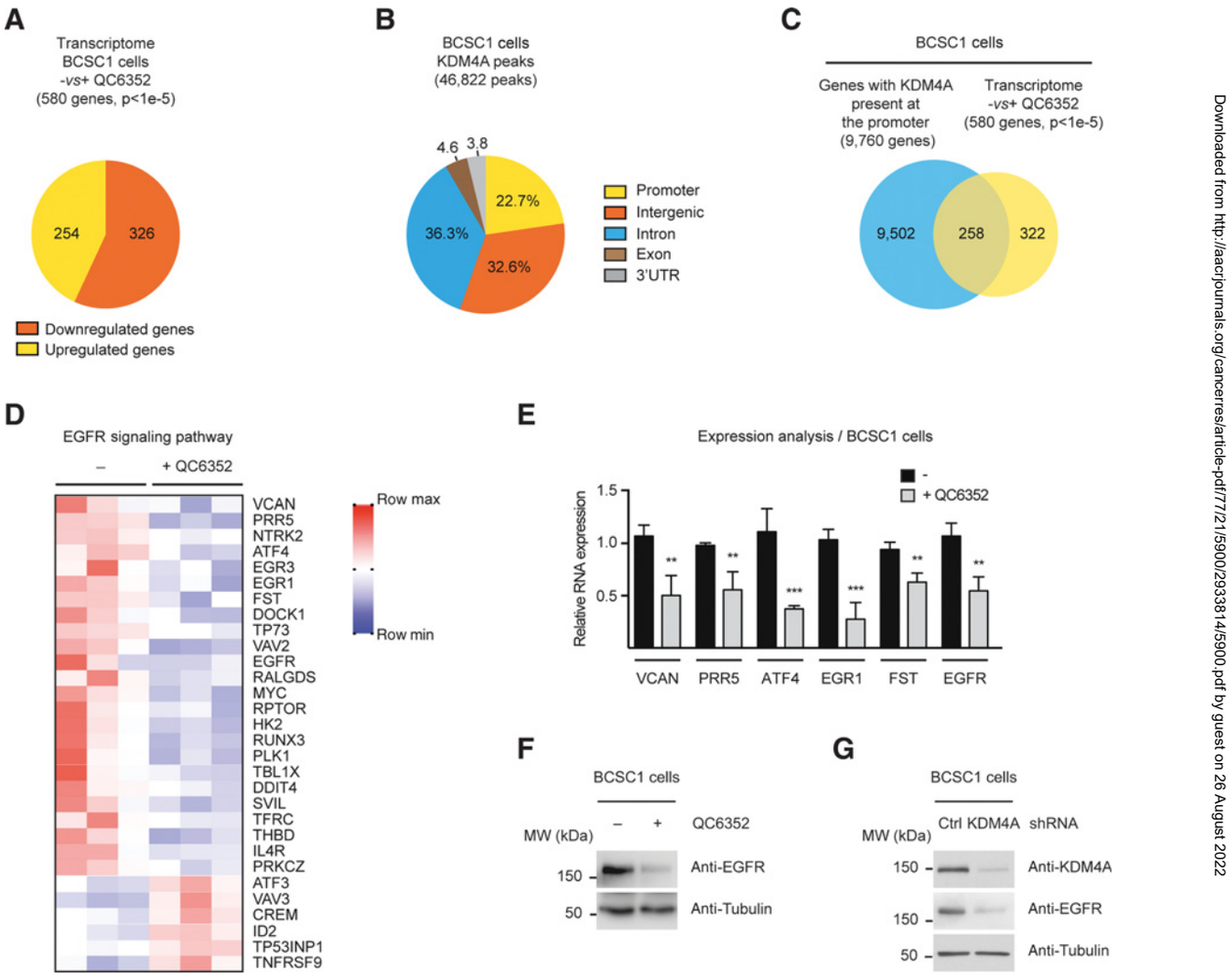

Figure 4.

QC6352 targets BCSCs through *EGFR* regulation. **A,** Pie chart displaying the number of genes that are differentially regulated in BCSC1 upon treatment with QC6352. **B,** Pie chart displaying genomic distribution of KDM4A in BCSC1 as determined by ChIP-seq analysis. **C,** Venn diagram showing the intersection and number of genes where KDM4A is present on the promoter region with genes that are differentially regulated in BCSC1 upon treatment with QC6352. A hypergeometric test was performed to calculate the significance of the overlap ($P < 10^{-50}$). **D,** mRNA level analysis. Heatmap representing the mRNA levels detected in BCSC1 cultured in the presence of vehicle (−) or QC6352. The 30 represented genes are direct target genes of KDM4A that belong to the "EGF receptor signaling pathway." **E,** Verification of transcriptome data. qRT-PCR analysis showing relative mRNA levels of indicated genes in BCSC1 cultured in the presence of vehicle (−) or QC6352 ($n = 4$). **F** and **G,** Anti-EGFR, anti-KDM4A, and anti-tubulin Western blots. Samples are lysates from BCSC1 cultured in the presence of vehicle (−) or QC6352 (**F**) or treated with control shRNA (shRNA Ctrl) or an shRNA against KDM4A (shRNA KDM4A; **G**). Data represent means + SD (**E**); **, $P < 0.01$; ***, $P < 0.001$ by two-tailed Student *t* test.

QC6352 targets BCSCs through *EGFR* regulation

To unravel the molecular mechanism underlying the action of the inhibitor, we performed transcriptome analyses to identify genes that were differentially regulated upon QC6352 treatment. BCSC1 were cultivated in the presence or absence of QC6352 and subjected to RNA-seq. Our analysis identified a total of 580 differentially regulated genes (Fig. 4A). Among them, 254 were upregulated and 326 were downregulated (Fig. 4A). To see whether these genes are direct KDM4A targets, we performed ChIP-seq in BCSC1 cells with anti-KDM4A antibody. The analysis shown in Fig. 4B identified 46,822 high confidence KDM4A peaks. *Motif analysis using HOMER* indicates enrichment of FOXA3, FOXL2, FOXA1, FOXP1, or FOXF1 motifs at KDM4A locations (Supplementary Fig. S4A). Only 3,221 (6.9%) KDM4A locations were observed in BCSC1 treated with shRNA against KDM4A, thus confirming specificity of the KDM4A antibody (Supplementary Fig. S4B). This finding prompted us to intersect the KDM4A cistrome with the QC6352 transcriptome. Among the 580 differentially regulated genes, KDM4A was present at the promoter of 258 genes (44%; Fig. 4C). Pathway analysis for these 258 genes revealed that 30 of these genes, including *EGFR*, belong to the "EGF receptor signaling pathway" (Fig. 4D). We verified by qRT-PCR analysis that treatment with QC6352 reduced the expression levels of genes such as *versican* (*VCAN*), *proline rich 5* (*PRR5*), *activating transcription factor 4* (*ATF4*), *early growth response 1* (*EGR1*), *follistatin* (*FST*), and importantly *EGFR* (Fig. 4E). EGFR is an emerging therapeutic target that is associated with poor clinical outcome of TNBC (28). To unravel the importance of EGFR signaling in growth of BCSCs we treated BCSC1 and BCSC2 with erlotinib, a specific EGFR inhibitor. Of note, treatment with erlotinib blocked proliferation of both BCSC1 and BCSC2 (Supplementary Fig. S4C–S4F). Furthermore, stem cell potential measured by anchorage-independent sphere-forming capacity of both BCSC1 and BCSC2 was dramatically reduced upon treatment with erlotinib (Supplementary Fig. S4G and S4H). Together, these data demonstrate that EGFR, at least in part, controls growth and stem cell potential of BCSCs. As shown by Western blot analysis, the protein levels of EGFR were reduced in both BCSC1 and BCSC2 upon treatment with QC6352 (Fig. 4F and Supplementary Fig. S4I). Because EGFR is a direct KDM4A target, we tested whether knockdown of KDM4A affects EGFR protein levels. As depicted in Fig. 4G and Supplementary Fig. S4J, shRNA-mediated knockdown of KDM4A led to reduced levels of EGFR in both BCSC1 and BCSC2. Of note, knockdown of KDM4B, C, or D in BCSC1 did not affect the levels of EGFR (Supplementary Fig. S4K–S4M). Taken together, the data show that EGFR expression in BCSCs is blocked by QC6352 via inhibition of KDM4A.

Because KDM4A is a demethylase that erases the repressive H3K9me3 mark, we hypothesized that an increase in H3K9me3 should be observed upon inactivation of KDM4A by QC6352. To this end, we performed genome-wide ChIP-seq with H3K9me3 antibody in BCSC1 cells that were treated with either vehicle or QC6352. To allow for normalization of H3K9me3 ChIP-seq tags, we added spike-in chromatin during the ChIP procedure (13). The analysis shown in Supplementary Fig. S5A identified 141,722 high confidence H3K9me3 peaks in vehicle-treated cells and

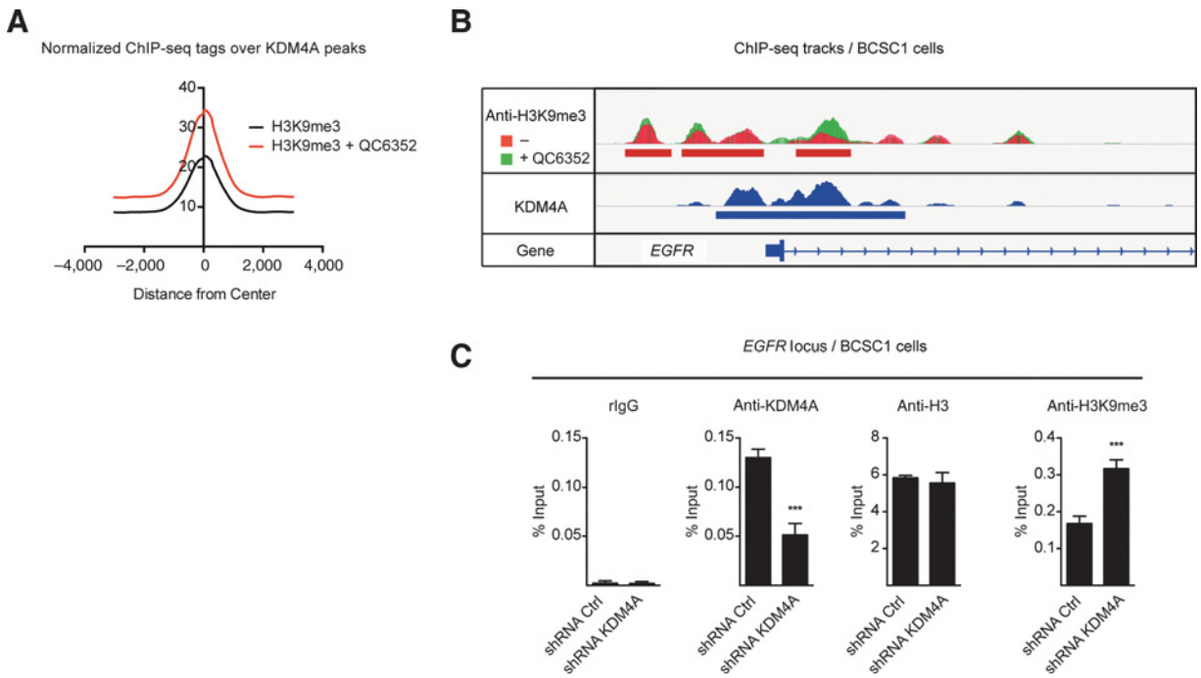

Figure 5.

Levels of H3K9me3 increase upon treatment with QC6352. **A,** Meta-analysis of sequencing read density based on H3K9me3 ChIP-seqs around KDM4A peaks in BCSC1 cultured in the presence of vehicle or QC6352. **B,** ChIP-Seq tracks. Normalized levels of H3K9me3 and KDM4A tracks at the *EGFR* promoter. **C,** ChIP analyses performed with anti-KDM4A, anti-H3, anti-H3K9me3, and rIgG. Samples originate from BCSC1 infected with an adenovirus coding either for shRNA Ctrl or shRNA KDM4A. The precipitated chromatin was quantified by qPCR using primers in the promoter region of the *EGFR* gene. Data represent means + SD (**C**); ***, $P < 0.001$ by two-tailed Student *t* test.

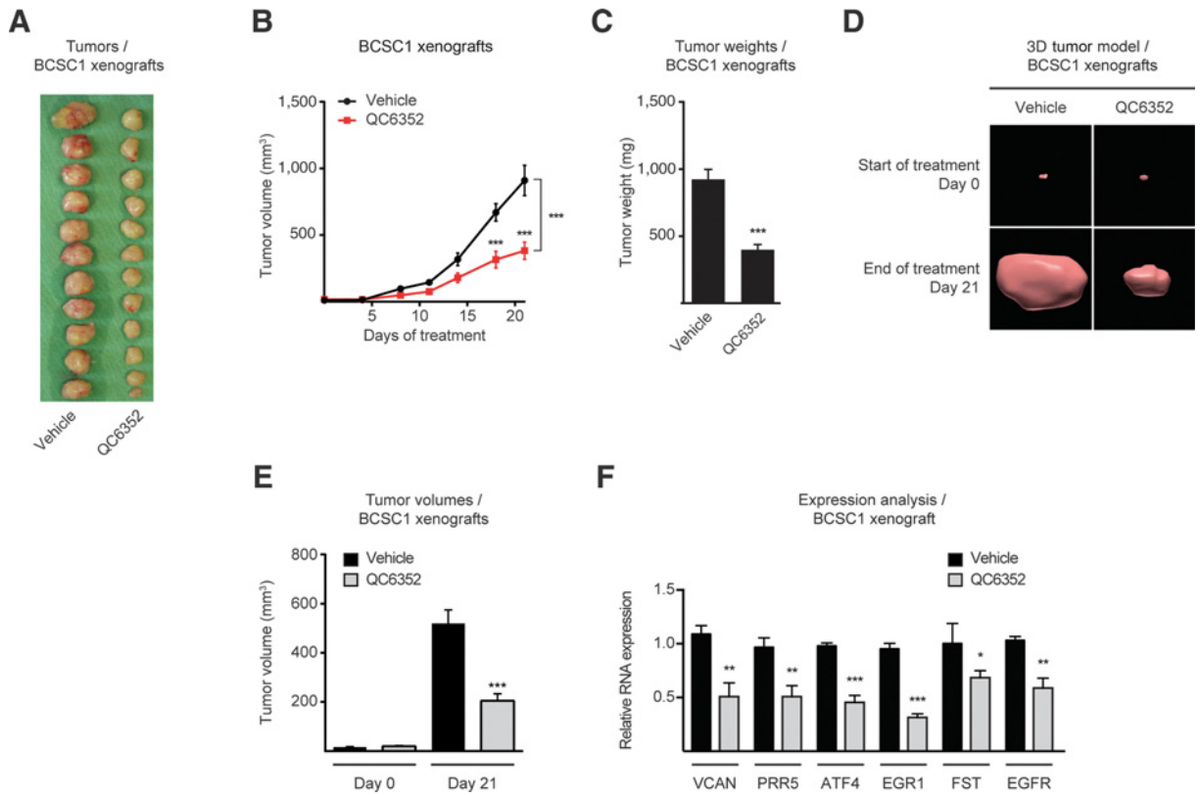

Figure 6.

QC6352 inhibits BCSC1-derived xenograft tumor growth. **A–E,** Mice bearing BCSC1 xenograft tumors were treated for 21 consecutive days with either vehicle or QC6352. **A,** Representative BCSC1 xenograft tumors isolated from individual animals after 21 days of treatment with either vehicle or QC6352. **B,** Increase in tumor volume was measured over time. **C,** Tumor weights after 21 days of treatment with vehicle or QC6352. **D** and **E,** Representative images of tumors (**D**) and volume quantification of all tumors (**E**) obtained by ultrasound imagery at the start (day 0) and after 21 days of treatment (day 21) with either vehicle or QC6352. For **A–E**: $n = 11$ (vehicle), $n = 12$ (QC6352). **F,** qRT-PCR analysis showing relative mRNA levels of indicated genes in BCSC1 xenograft tumors of mice treated with either vehicle or QC6352 ($n = 4$). Data represent means ± SEM (**B**), means + SEM (**C** and **E**), or means + SD (**F**); *, $P < 0.05$; **, $P < 0.01$; ***, $P < 0.001$ by one-way ANOVA (**B**, **C** and **E**) or two-tailed Student *t* test (**F**).

144,266 peaks in cells treated with QC6352. Importantly, we observed a global increase of the H3K9me3 reads over the KDM4A peaks (Fig. 5A). Similarly, on the *EGFR* promoter we also observed increased levels of the repressive H3K9me3 mark over the KDM4A peak subsequent to inactivation by QC6352 (Fig. 5B). To demonstrate that the increase of H3K9me3 levels at the *EGFR* promoter upon treatment with QC6352 is due to inhibition of KDM4A, we infected BCSC1 cells with adenovirus encoding either shRNA control (shRNA Ctrl) or shRNA against KDM4A (shRNA KDM4A) and performed ChIP assays. ChIP-qPCR analyses indicate that in BCSC1 infected with shRNA KDM4A the levels of H3K9me3 at the *EGFR* promoter increase concomitantly to a decrease in KDM4A when compared to control cells (Fig. 5C). In summary, these results demonstrate that treatment of BCSCs with QC6352 targets *EGFR* via inhibition of the KDM4A demethylase activity.

QC6352 inhibits BCSC-derived xenograft tumor growth

Next, we wondered whether QC6352 might affect growth of BCSC1 and BCSC2 xenografts. Therefore, 1×10^5 cells were implanted into the fat pads of immunocompromised NOD/SCID mice. To mimic the clinical treatment situation of a preexisting tumor we allowed growth of the xenografts to a size of 3 mm^3 before starting treatment. Mice carrying tumors were then treated with QC6352 for 21 days at 10 mg/kg per os. Importantly, QC6352 strongly affected tumor growth and final tumor weight of both BCSC1 and BCSC2 xenografts (Fig. 6A–E and Supplementary Fig. S6A–S6E). Treatment with QC6352 was well tolerated and did not affect body weight of the mice (Supplementary Fig. S6F and S6G). Furthermore, we analyzed whether treatment with QC6352 affected expression of KDM4A target genes in the BCSC1 xenograft tumors in a similar manner as observed in cell culture (Fig. 4E). As displayed in Fig. 6F, expression of *VCAN*, *PRR5*, *ATF4*, *EGR1*, *FST*, and *EGFR* was similarly affected in BCSC1 xenograft tumors of QC6352-treated mice as *in vitro*. Taken together, our data demonstrate that treatment with the KDM4 inhibitor QC6352 blocks BCSC xenograft tumor growth.

Discussion

In recent years, CSCs from solid tumors were identified using surface marker profiles and subsequent limiting dilution orthotopic xenografts. The first description of BCSCs by Al-Hajj and colleagues identified that the BCSC population is marked by

$CD24^{low}/CD44^{high}$ cells (24). In addition, several other surface molecules such as CD61, CD49f, and EpCAM identifying BCSCs were proposed (29, 30). Importantly, due to a lack of appropriate culture conditions BCSCs cannot be cultivated continuously *in vitro* in a stem cell state (31, 32). To address this issue and to stabilize the CSC phenotype, we used a 3D Matrix and applied a Rho Kinase inhibitor in a low oxygen environment. Thus, our culture conditions allowed cultivation of BCSCs directly from the patient tumor without the need for initial separation of tumor tissue and CSCs by FACS or the expansion of the patient's tumor tissue in murine xenografts. Limiting dilution transplants of our cultivated BCSCs regenerated the original patient's tumor. The xenograft tumors had an almost identical immunohistochemical pattern compared with the tumor of origin, which is comparable to results obtained from direct patient xenografts (24, 33). In addition, transcriptome analyses uncovered a strong clustering of primary tumors, xenografts, and cell lines. Thus, BCSCs faithfully reproduce the original patient's tumor and are therefore an ideal cellular platform to test novel therapeutics.

Because breast cancer progression was shown to be associated with alterations of KDM4 demethylase family members (8, 34–36), we set out to characterize the expression profiles of the four KDM4 family members, namely KDM4A, B, C, and D in BCSC1 and BCSC2. BCSC1 and BCSC2 are characterized by a robust expression of KDM4A. In contrast, expression levels of KDM4B, C, and D were more heterogeneous. While depletion of KDM4A impaired proliferation of BCSC1 and blocked growth of BCSC1 tumor xenografts, knockdown of the other KDM4 family member neither affected cell proliferation nor xenograft tumor growth. These findings are in accordance with previous studies suggesting that KDM4A controls proliferation of breast cancer cells (37, 38). Furthermore, by showing for the first time that KDM4A controls proliferation and self-renewal of BCSCs isolated from chemotherapy-resistant triple-negative breast tumors we validate KDM4A as a therapeutic target.

In recent years diverse KDM4 inhibitors have been identified, which act either as α-ketoglutarate mimics, a cofactor essential for the enzymatic function of KDM4s, or as inhibitors of the catalytic site (8). These molecules showed inhibitory effects on KDM4s *in vitro* and in cell culture models (8). However, these KDM4 inhibitors did not qualify as therapeutic agents. In contrast, QC6352 is a drug-like KDM4 inhibitor that is potent, selective, orally available and presents favorable pharmacokinetic properties.

In summary, we established an advanced culture method that allows isolation and growth of BCSC lines isolated from individual patient tumors after neoadjuvant chemotherapy. We demonstrate that BCSC xenografts faithfully recapitulate parental patient tumors and that BCSCs, BCSC xenografts, and the parental tumors share a highly similar transcriptome and phenotype profile. Therefore, our models are ideal tools for the identification and validation of novel therapeutics. In line with this idea, we identified the histone demethylase KDM4A as a therapeutic target for BCSC-originating tumors. Consequently, we showed that the orally available, potent, and selective KDM4 inhibitor QC6352 abrogates expression of target genes via inhibition of the KDM4A demethylase activity, thereby blocking proliferation, sphere-forming capacity *in vitro*, and xenograft tumor growth of BCSCs *in vivo*. Thus, modulation of KDM4 activity is a promising therapeutic strategy for the treatment of TNBC.

Disclosure of Potential Conflicts of Interest

R. Schüle is a consultant/advisory board member for Celgene. No potential conflicts of interest were disclosed by the other authors.

Authors' Contributions

Conception and design: E. Metzger, J. Xu, M.B. Wallace, J. Maurer, R. Schüle
Development of methodology: E. Metzger, S.S. Stepputtis, B.-T. Preca, M. Follo, T. Kanouni, J. Maurer, R. Schüle
Acquisition of data (provided animals, acquired and managed patients, provided facilities, etc.): E. Metzger, S.S. Stepputtis, J. Strietz, D. Willmann, A. Allen, P. Bronsert, E. Stickeler, J. Maurer, R. Schüle
Analysis and interpretation of data (e.g., statistical analysis, biostatistics, computational analysis): E. Metzger, S.S. Stepputtis, J. Strietz, B.-T. Preca, D. Willmann, N. Iovino, M. Follo, M. Boerries, J. Xu, J. Maurer, R. Schüle
Writing, review, and/or revision of the manuscript: E. Metzger, S.S. Stepputtis, J. Xu, M.B. Wallace, J.A. Stafford, T. Kanouni, J. Maurer, R. Schüle
Administrative, technical, or material support (i.e., reporting or organizing data, constructing databases): E. Metzger, S. Urban, D. Willmann, F. Zenk, A. Proske, E. Stickeler, J. Maurer, R. Schüle
Other (design and synthesis of QC6352): M.B. Wallace

Acknowledgments

We thank Hauke Busch for expert advice and help with bioinformatics analyses. Furthermore, we thank Robert Oshima and Pedro Aza-Blanc for providing reagents and the ZTZ Core Facility for expert advice and technical support. We are obliged to Astrid Rieder, Jessica Pfannstiel, Lisa Füner, and Bettina Herde for providing excellent technical assistance.

Grant Support

This work was supported by grants of the European Research Council (ERC AdGrant 322844) and the Deutsche Forschungsgemeinschaft SFB 992, 850, 746 to R. Schuele and by Deutsche Forschungsgemeinschaft SFB 850 and funding by DKTK to J. Maurer and M. Boerries. M. Boerries is funded by the German Federal Ministry of Education and Research within the framework of the e:Med research and funding concept, DeCaRe (FKZ 01ZX1409B).

The costs of publication of this article were defrayed in part by the payment of page charges. This article must therefore be hereby marked *advertisement* in accordance with 18 U.S.C. Section 1734 solely to indicate this fact.

Received June 22, 2017; revised August 5, 2017; accepted September 1, 2017; published OnlineFirst September 7, 2017.

References

1. Ferlay J, Soerjomataram I, Ervik M, Dikshit R, Eser S, Mathers C, et al. GLOBOCAN 2012 v1.0, Cancer Incidence and Mortality Worldwide: IARCCancerBase No. 112013.
2. Kim JE, Ahn HJ, Ahn JH, Yoon DH, Kim SB, Jung KH, et al. Impact of triple-negative breast cancer phenotype on prognosis in patients with stage I breast cancer. J Breast Cancer 2012;15:197–202.
3. Reya T, Morrison SJ, Clarke MF, Weissman IL. Stem cells, cancer, and cancer stem cells. Nature 2001;414:105–11.
4. Shaw C, Wilkinson M, Cynader M, Needler MC, Aoki C, Hall SE. The laminar distributions and postnatal development of neurotransmitter and neuromodulator receptors in cat visual cortex. Brain Res Bull 1986;16:661–71.
5. Ye Q, Holowatyj A, Wu J, Liu H, Zhang L, Suzuki T, et al. Genetic alterations of KDM4 subfamily and therapeutic effect of novel demethylase inhibitor in breast cancer. Am J Cancer Res 2015;5:1519–30.
6. Berry WL, Janknecht R. KDM4/JMJD2 histone demethylases: epigenetic regulators in cancer cells. Cancer Res 2013;73:2936–42.
7. Whetstine JR, Nottke A, Lan F, Huarte M, Smolikov S, Chen Z, et al. Reversal of histone lysine trimethylation by the JMJD2 family of histone demethylases. Cell 2006;125:467–81.

8. Labbe RM, Holowatyj A, Yang ZQ. Histone lysine demethylase (KDM) subfamily 4: structures, functions and therapeutic potential. Am J Transl Res 2013;6:1–15.
9. Castro F, Dirks WG, Fahnrich S, Hotz-Wagenblatt A, Pawlita M, Schmitt M. High-throughput SNP-based authentication of human cell lines. Int J Cancer 2013;132:308–14.
10. Metzger E, Wissmann M, Yin N, Muller JM, Schneider R, Peters AH, et al. LSD1 demethylates repressive histone marks to promote androgen-receptor-dependent transcription. Nature 2005;437:436–9.
11. Langmead B, Trapnell C, Pop M, Salzberg SL. Ultrafast and memory-efficient alignment of short DNA sequences to the human genome. Genome Biol 2009;10:R25.
12. Zhang Y, Liu T, Meyer CA, Eeckhoute J, Johnson DS, Bernstein BE, et al. Model-based analysis of ChIP-Seq (MACS). Genome Biol 2008;9:R137.
13. Orlando DA, Chen MW, Brown VE, Solanki S, Choi YJ, Olson ER, et al. Quantitative ChIP-Seq normalization reveals global modulation of the epigenome. Cell Rep 2014;9:1163–70.
14. Thorvaldsdottir H, Robinson JT, Mesirov JP. Integrative Genomics Viewer (IGV): high-performance genomics data visualization and exploration. Brief Bioinform 2013;14:178–92.
15. Heinz S, Benner C, Spann N, Bertolino E, Lin YC, Laslo P, et al. Simple combinations of lineage-determining transcription factors prime cis-regulatory elements required for macrophage and B cell identities. Mol Cell 2010;38:576–89.
16. Dunning MJ, Smith ML, Ritchie ME, Tavare S. beadarray: R classes and methods for Illumina bead-based data. Bioinformatics 2007;23:2183–4.
17. Wolff AC, Hammond ME, Schwartz JN, Hagerty KL, Allred DC, Cote RJ, et al. American Society of Clinical Oncology/College of American Pathologists guideline recommendations for human epidermal growth factor receptor 2 testing in breast cancer. Arch Pathol Lab Med 2007;131:18–43.
18. Goldhirsch A, Winer EP, Coates AS, Gelber RD, Piccart-Gebhart M, Thurlimann B, et al. Personalizing the treatment of women with early breast cancer: highlights of the St Gallen International Expert Consensus on the Primary Therapy of Early Breast Cancer 2013. Ann Oncol 2013;24:2206–23.
19. Metzger E, Willmann D, McMillan J, Forne I, Metzger P, Gerhardt S, et al. Assembly of methylated KDM1A and CHD1 drives androgen receptor-dependent transcription and translocation. Nat Struct Mol Biol 2016;23:132–9.
20. Metzger E, Imhof A, Patel D, Kahl P, Hoffmeyer K, Friedrichs N, et al. Phosphorylation of histone H3T6 by PKCbeta(I) controls demethylation at histone H3K4. Nature 2010;464:792–6.
21. Trapnell C, Roberts A, Goff L, Pertea G, Kim D, Kelley DR, et al. Differential gene and transcript expression analysis of RNA-seq experiments with TopHat and Cufflinks. Nat Protoc 2012;7:562–78.
22. Robinson MD, Smyth GK. Small-sample estimation of negative binomial dispersion, with applications to SAGE data. Biostatistics 2008;9:321–32.
23. Beck B, Blanpain C. Unravelling cancer stem cell potential. Nat Rev Cancer 2013;13:727–38.
24. Al-Hajj M, Wicha MS, Benito-Hernandez A, Morrison SJ, Clarke MF. Prospective identification of tumorigenic breast cancer cells. Proc Natl Acad Sci U S A 2003;100:3983–8.
25. Castro DJ, Maurer J, Hebbard L, Oshima RG. ROCK1 inhibition promotes the self-renewal of a novel mouse mammary cancer stem cell. Stem Cells 2013;31:12–22.
26. Chen YK, Bonaldi T, Cuomo A, Del Rosario JR, Hosfield DJ, Kanouni T, et al. Design of KDM4 inhibitors with antiproliferative effects in cancer models. ACS Med Chem Lett 2017;8:869–74.
27. Duteil D, Tosic M, Lausecker F, Nenseth HZ, Muller JM, Urban S, et al. Lsd1 ablation triggers metabolic reprogramming of brown adipose tissue. Cell Rep 2016;17:1008–21.
28. Hsu JL, Hung MC. The role of HER2, EGFR, and other receptor tyrosine kinases in breast cancer. Cancer Metastasis Rev 2016;35:575–88.
29. Scheel C, Eaton EN, Li SH, Chaffer CL, Reinhardt F, Kah KJ, et al. Paracrine and autocrine signals induce and maintain mesenchymal and stem cell states in the breast. Cell 2011;145:926–40.
30. Stingl J, Eaves CJ, Zandieh I, Emerman JT. Characterization of bipotent mammary epithelial progenitor cells in normal adult human breast tissue. Breast Cancer Res Treat 2001;67:93–109.
31. Gjorevski N, Sachs N, Manfrin A, Giger S, Bragina ME, Ordonez-Moran P, et al. Designer matrices for intestinal stem cell and organoid culture. Nature 2016;539:560–4.
32. Bartfeld S, Clevers H. Stem cell-derived organoids and their application for medical research and patient treatment. J Mol Med (Berl) 2017;95:729–38.
33. DeRose YS, Wang G, Lin YC, Bernard PS, Buys SS, Ebbert MT, et al. Tumor grafts derived from women with breast cancer authentically reflect tumor pathology, growth, metastasis and disease outcomes. Nat Med 2011;17:1514–20.
34. Chu CH, Wang LY, Hsu KC, Chen CC, Cheng HH, Wang SM, et al. KDM4B as a target for prostate cancer: structural analysis and selective inhibition by a novel inhibitor. J Med Chem 2014;57:5975–85.
35. Qiu MT, Fan Q, Zhu Z, Kwan SY, Chen L, Chen JH, et al. KDM4B and KDM4A promote endometrial cancer progression by regulating androgen receptor, c-myc, and p27kip1. Oncotarget 2015;6:31702–20.
36. Soini Y, Kosma VM, Pirinen R. KDM4A, KDM4B and KDM4C in non-small cell lung cancer. Int J Clin Exp Pathol 2015;8:12922–8.
37. Li BX, Zhang MC, Luo CL, Yang P, Li H, Xu HM, et al. Effects of RNA interference-mediated gene silencing of JMJD2A on human breast cancer cell line MDA-MB-231 in vitro. J Exp Clin Cancer Res 2011;30:90.
38. Li BX, Luo CL, Li H, Yang P, Zhang MC, Xu HM, et al. Effects of siRNA-mediated knockdown of jumonji domain containing 2A on proliferation, migration and invasion of the human breast cancer cell line MCF-7. Exp Ther Med 2012;4:755–61.